Polymer Chemistry

PAPER

Classical photopolymerization kinetics, exceptional gelation, improved diffraction efficiency and driving voltage in scaffolding morphological H-PDLCs afforded by photoinitibitor

Haiyan Peng,*[,a,b,d] Guannan Chen,[c] Mingli Ni,[c] Yan Yan,[b] Jiaqing Zhuang,[b] V. A. L. Roy,[b] Robert K Y Li[b] and Xiaolin Xie*[,c,e]

Holographic polymer dispersed liquid crystals (H-PDLCs) pertain to one type of intriguing switchable electro-optical devices, and it is a constant need to quantitatively understand the photopolymerization kinetics and gelation during the formation of H-PDLCs for the purpose of improving the diffraction efficiency and driving voltage. Herein, we quantitatively investigate the effect of the photoinitibitor composed of 3,3'-carbonylbis(7-diethylaminocoumarin) (KCD) and *N*-phenylglycine (NPG), with initiation and inhibition functions simultaneously generated under monochromatic illumination, on the formation of H-PDLCs. The outcomes reveal that an augment of KCD loading from 0.3×10^{-3} to 1.4×10^{-3} mol/L dramatically promotes the photopolymerization rate and monomer conversion. Reversely, a further increase of KCD content drastically depresses the photopolymerization. Numerical deduction shows that the kinetics complies with the classical photopolymerization kinetics characteristics in the full range of KCD content. Counterintuitively, the gelation time almost keeps constant when the KCD content is less than 1.8×10^{-3} mol/L, and then is able to grow by more than 4 times when further increasing the KCD loading. The ketyl radical inhibition, which subsequently results in shortened weight-average chain lengths and increased gel point conversions, is believed to account for the kinetics and exceptional gelation behaviors. H-PDLCs with scaffolding morphology are formed, and with an augment of KCD content, the segregation degree and diffraction efficiency significantly improve from zero to 64% and 78±11%, respectively, and then level off, allowing for the facile fabrication of glasses-free colored 3D images; while the critical driving voltage gradually decreases from 8.9 ± 1.0 to 4.6 ± 0.7 V/μm.

Introduction

Photopolymerization, which is a simple, facile and versatile technique capable of converting functional small molecules in liquid to solid polymer parts by taking advantage of light, represents an impressive variety of advantageous characteristics such as fast reaction speed, mild reaction conditions, the ability to solvent-free processing as well as the amenability for spatiotemporal polymerization manipulation. Numerous protocols with elegant designs based on photo-mediated reactions have been established and are technically useful in a vast range of scientific and industrial realms, such as electronics, optics, electro-optical devices, patterning, printing, bio-scaffolds, adhesives, sealants and coatings.[1-8] By integrating with the additive manufacturing technique known as three-dimensional (3D) printing, photopolymerization is also able to enable the fast fabrication of complex 3D objects with desirable features and characteristics.[9, 10] In general, photopolymerization occurs under light exposure *via* several sequential steps, *i.e.*, photon absorption by sensitizers, generation of initiating species (radicals, anions or cations), subsequent initiation, propagation and termination. No matter what kind of initiating species one employs to trigger the photopolymerization, it is critical to implement spatial and/or temporal control over the photopolymerization kinetics and/or gelation process with satisfactory precision, for an aim of controlling the monomer conversion, polymer molecular weight and weight distributions[11, 12], nanostructure,[13] architecture[14], thermal and mechanical characteristics,[15, 16] optical properties,[17, 18], and so forth. Toward this end, one strategy that employs photo-mediated initiation and inhibition emerges and could have the great potential to be more robust and adaptable than other techniques to realize the ease of spatiotemporal control over the photopolymerization.[9, 19-23] For instance, Scott and co-workers have enabled subdiffraction photolithography through two-color single-photon initiation

a. *Shenzhen Institutes of Advanced Technology, Shenzhen 518055, China. E-mail: hy.peng@giat.ac.cn*
b. *Department of Physics and Materials Science, City University of Hong Kong, Tat Chee Avenue, Kowloon Tong, Hong Kong SAR, China*
c. *Key Lab for Large-Format Battery Materials and Systems, Ministry of Education, School of Chemistry and Chemical Engineering, Huazhong University of Science and Technology, Wuhan 430074, China. E-mail: xlxie@mail.hust.edu.cn*
d. *Guangzhou Institute of Advanced Technology, Chinese Academy of Sciences, Guangzhou 511458, China*
e. *National Anticounterfeit Engineering Research Center, Huazhong University of Science and Technology, Wuhan 430074, China*

ARTICLE   **Polymer Chemistry**

and inhibition.[19] In detail, they irradiated a visible light sensitive initiator, composed of camphorquinone and ethyl 4-(dimethylamino)benzoate by a 473 nm Gaussian laser beam to start the photopolymerization, while activating the inhibitor named tetraethylthiuram disulfide to terminate the polymerization by a 364 nm UV laser in the mode of Gauss-Laguerre "doughnut". The superimposed regions of the two laser beams with prolonged gelation then could be readily washed away by solvents, with solid polymer parts left in a reduced size in the focal point of the Gaussian visible beam.[19] On the basis of this ingenious design, Gan and co-workers have created small features with a size down to 9 nm.[21] Another innovative paradigm employing inhibition is also amazing in which, through creating an oxygen-containing "dead zone" to terminate the photopolymerization, Tumbleston and co-workers have realized continuous manufacturing of complex 3D objects such as an Eiffel Tower model by 3D printing at rates of tens of centimeters per hour.[9] This technique is talented since oxygen inhibition is generally a serious concern in radical chain-growth photopolymerization and thus required to be eliminated in traditional procedures.[24, 25] Distinct from the two approaches aforementioned, our group has recently proposed a novel photoinitibitor in which, one radical for initiation and another for inhibition are simultaneously generated under monochromatic visible light irradiation.[22] This photoinitibitor is able to improve the phase separation and diffraction efficiency of either holographic polymer dispersed liquid crystals (H-PDLCs) or photopolymer/ZnS nanocomposites.[19,20] We focused on the visible light active photopolymerization because it is much safer, more energy-efficient to manipulate than UV light.[26, 27] One typical photoinitibitor is composed of a sensitizer 3,3'-carbonylbis(7-diethylaminocoumarin) (KCD) and a co-initiator *N*-phenylglycine (NPG), as shown in Scheme 1. Since dye radicals, *e.g.* ketyl radicals, involved in photopolymerization were regarded to be detrimental and thus required to be scavenged previously,[8, 25, 28] the newly disclosed photoinitibitor seems to realize new positive perspectives on the application of dye radicals. Nevertheless, the exploration of photoinitibitor is still in its infancy, and the quantitative understanding of concentration-dependent photopolymerization kinetics, gelation, phase separation and holographic performances is unexplored and highly awaited for the formulation optimization purpose. Meanwhile, the pioneering work may raise a question of whether the diffraction enhancement is dominated by the depressed reaction in light of Beer-Lambert Law, since fine holographic gratings are able to form *via* either increasing the dye loading,[22, 23] or decreasing the light intensity,[23] thus deeper investigations are in urgent need.

Holography is a technically useful interference process by multiple coherent laser beams, with holograms generated in line with the sinusoidal distribution of both amplitude and phase information of the light employed. It has been known that holography is able to exhibit unique and fantastic attributes such as immense data storage with a density up to gigabits per cubic centimeter, fast data transfer speed in nanoseconds, page-wise readout characteristic, and capability of random data processing in three dimensions with minimal cross-talk.[29, 30] As such, holograms offer great potentials to function as devices for broad applications such as colored 3D image storage,[22, 23, 31] glasses-free 3D dynamic display,[32, 33] graded rainbow patterning,[17, 34] and optically responsive sensing.[35]
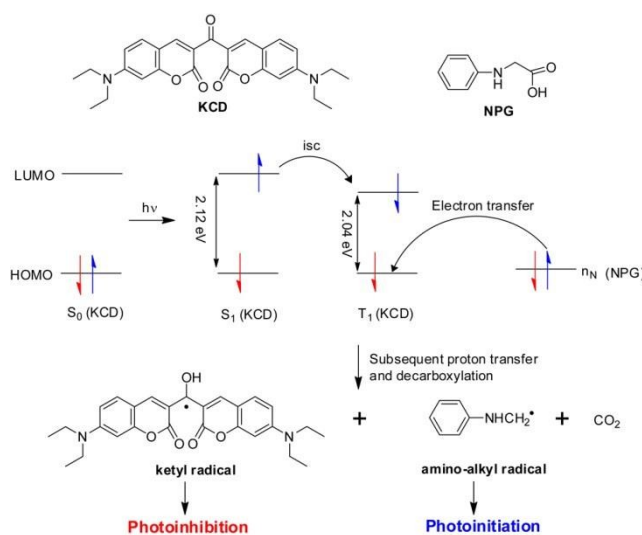
Scheme 1 Proposed reaction mechanism of the photoinitibitor composed of KCD and NPG under light irradiation.

Among all holograms, holographic polymer dispersed liquid crystals (H-PDLCs), pioneered by Sutherland and co-workers in 1993,[36, 37] have drawn extensive research interest because of their fantastic switchable electro-optical properties, and their great application potentials in biomedical tunable-filters,[38] organic distributed feedback lasers,[39, 40] optically switchable photonic structures,[41] displays,[42, 43] and so forth. H-PDLCs are typically formed *via* photopolymerization induced phase separation, *i.e.*, photopolymerization takes place in the bright regions of interference patterns, resulting in a chemical potential difference between the bright and dark regions. Subsequently, monomers are driven to diffuse from dark regions to bright regions to form polymers, while LCs are squeezed from bright areas to dark areas to form LC-rich domains, finally yielding a sinusoidal distribution of materials and corresponding refractive indices.[22, 37, 44-46] Non-droplet scaffolding morphology is expected to offer high diffraction efficiency in H-PDLCs as the phase separation is envisioned to be enhanced and the light scattering is depressed.[46-50] Nevertheless, H-PDLCs with high diffraction efficiency is not necessary to offer low driving voltage, and the high driving voltage is expected to limit the practical applications of H-PDLCs. For instance, De Sarkar and co-workers have investigated the effect of monomer average functionality on the properties of H-PDLCs, and realized that the diffraction efficiency reaches its peak when the monomer average functionality is 1.5, but the driving voltage increases dramatically with a decrease of monomer average

functionality. Adding surfactants is shown to be an efficient approach to decrease the driving voltage as the surfactants are able to decrease the interface interaction, yet the segregation degree is observed to be decreased because of the increased miscibility between polymers and LCs.[51-53] Alternatively, employing siloxane polymers[54] or fluorinated polymers[55] is shown to be efficient to simultaneously increase the diffraction efficiency and decrease the driving voltage as these polymers are able to decrease the miscibility of polymers and LCs, and thus capable of increasing the phase separation. Nevertheless, the choice of these siloxane or fluorinated polymers with low surface energy is limited and thus novel approaches are highly awaited.

Herein, to get a deeper insight into the photoinitibitor, and to answer the significant aforementioned questions, we employ the photoinitibitor, composed of KCD and NPG, to investigate the concentration dependent photopolymerization kinetics, gelation, phase separation, and electro-optical behaviors of H-PDLCs, with numerical expressions established to describe these fundamental reaction-structure-property relationships.

Experimental

Materials

N-vinylpyrrolidone (NVP, purity: 99%) and *N*-phenylglycine (NPG) were purchased from Aldrich and Aladdin, respectively. 2-ethylhexyl acrylate (EHA, purity: > 99%) and 3,3'-carbonylbis(7-diethylaminocoumarin) (KCD, purity: 99%) were obtained from Acros Organics. The LCs mixture named P0616A (Δn = 0.20, $n_{e(589nm, 293 K)}$ =1.72, T_{NI} = 331 K) was commercial available from Shijiazhuang Chengzhi Yonghua Display Material Co., Ltd., China. The hyperbranched acrylate monomer named 6361-100 was supported as a gift by Eternal Chemical Co., Ltd., China.

Preparation of holographic mixtures

Table 1 Varied KCD concentrations in the holographic mixtures.

Entry	KCD (10^{-3} mol/L)	Entry	KCD (10^{-3} mol/L)
1#	0.3	7#	8.2
2#	0.9	8#	11.0
3#	1.4	9#	13.7
4#	1.8	10#	16.4
5#	2.8	11#	19.1
6#	5.5	12#	21.8

Homogeneous mixtures for holography were prepared under ultrasonication at 323 K for 1 h. KCD, NPG and NVP were first added into a brown glass bottle with a sealed cap, and ultrasonically mixed for 50 min. Then other chemicals were added into the bottle, followed by another 10 min

ultrasonication. The weight ratio of EHA, NVP, 6361-100, P0616A and NPG was kept at 18: 9: 25: 26: 1 as determined before,[46] while the KCD concentrations were allowed to vary from 0.3×10^{-3} to 21.8×10^{-3} mol/L, as shown in **Table 1**.

Photopolymerization kinetics

The photopolymerization kinetics was investigated by a photo-differential scanning calorimeter (P-DSC, TA instruments, Q2000). Around 10 mg liquid holographic mixture was added into an aluminum-pan with a micropipette, and then the plan with samples and another empty one as the reference were located on two separate DSC sample holders. After being kept at 303 K for 5 min under a nitrogen gas protection with a constant purge rate of 50 mL/min, these two pans were isothermally irradiated from the top for 20 min by two separate monochromatic light beams at the wavelength of 442 nm, with an equal intensity of 20 mW/cm^2 for each respectively. The calculation of polymerization rate and double bond conversion was implemented *via* the previously reported method.[22, 46]

Photorheology characterization

Both storage and loss moduli for holographic mixtures during photopolymerization were *in-situ* monitored using a rheometer (Anto-Paar, MCR 302). Two parallel plates, 25 mm in diameter, were employed to sandwich the liquid sample with a thickness of 0.1 mm, where the bottom plate was transparent polyester that enabled the transmission of visible light. Strain sweeps were performed during the characterization with 0 N of normal force, 10 rad/s of angular frequency and 15% of strain amplitude. Before light exposure, the samples were kept in equilibrium at 303 K for 10 s. Subsequently, the samples were isothermally irradiated using a monochromatic 442 nm light source with an intensity of 20 mW/cm^2. A flow of nitrogen gas was continuously purged at a rate of 50 mL/min to prevent oxygen inhibition.

Holograms fabrication

For holographic recording, the holographic mixtures were sandwiched into a LC cell with ITO coated inner surfaces and a cell gap of ~10 μm. A splitter was used to divide the incident 442 nm He-Cd laser into two separate beams with an equal intensity of 10 mW/cm^2 for each individually, and then these two beams simultaneously irradiated the prepared LC cells at an external angle of ~31°. The bisector of the two beams was set normal to the cell plane, allowing for the generation of unslanted interference patterns with a period of ~827 nm according to the Bragg condition. Finally, post-curing was employed on these cells after holographic recording to solidify the holograms by using a mercury lamp. Colored 3D images were replicated through the method as previously reported.[22] In detail, one 442 nm laser beam was divided into two beams by a splitter and then expanded separately using two beam expanders. One of these two beams directly irradiated the H-PDLCs recording plate as the reference beam, while another beam, as the object beam, first irradiated a master that stored a 3D image and generated one diffraction beam. Subsequently, the diffraction beam and the reference beam interfered in the H-PDLCs material, consequently replicated the 3D image that was originally stored in the master. The total light intensity of these two beams reaching the H-PDLCs was around 1 mW/cm^2 and the recording

time was 300 s. This image replication method could avoid image blurring by significantly decreasing the distance between the image and the recording plate, offering visually recognizable images to the naked eye under white light illumination.

Electro-optical measurements

LC cells with interference patterns were mounted on the sample stage of LCT-5016C display parameter tester (North LC Engineering Research and Development Centre, China), and then probed by a highly collimated p-polarized 633 nm He-Ne laser (Thorlabs, USA) at the Bragg angle for implementing the non-constructive diffraction efficiency characterization. Diffraction efficiency was determined as the ratio of first-order diffraction intensity to the total intensities of transmitted and diffracted beams. A square wave voltage with a frequency of 1 kHz, which consecutively ramped from zero to 150 V during test at a step of 0.5 V, was applied to switch the H-PDLCs gratings. Four different samples for each entry were tested, and average values with errors were given in the text.
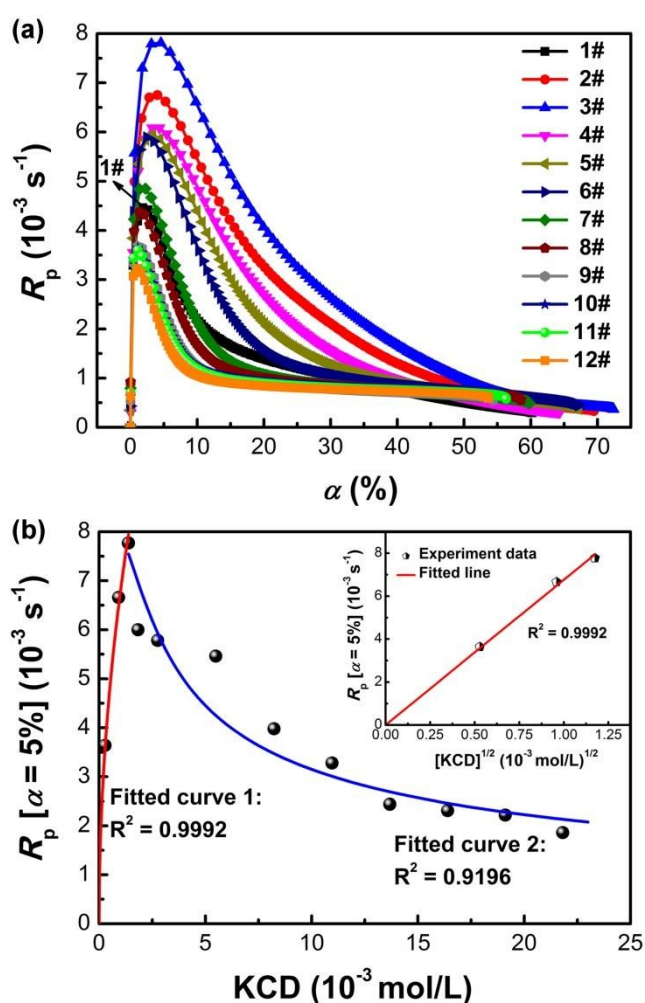

Fig. 1 KCD concentration dependent photopolymerization kinetics. (a) Polymerization rate, R_p, as a function of double band conversion, α, at varied concentrations of KCD. The KCD concentrations for each entry are listed in Table 1. (b) R_p versus KCD concentration when the α reaches 5%. Inset: R_p is linearly proportional to the square root of KCD concentration when the KCD content is less than 1.4×10^{-3} mol/L.

Morphology characterization

The LC cells with interference patterns were cut into small specimens, which were then immersed in analytical pure n-hexane for 48 h to extract LCs from the gratings, followed by drying in air and coating with a thin layer of platinum. The grating surface morphology of the prepared samples was characterized by a field emission scanning electron microscope (FESEM, Sirion 200).

Results and discussion

To get a quantitative understanding of the effect of photoinitibitor concentration on the photopolymerization kinetics, gelation, phase separation and electro-optical behaviors of H-PDLCs gratings, we herein vary the KCD concentrations from 0.3×10^{-3} to 21.8×10^{-3} mol/L, while letting the NPG content be kept constant. We choose NPG as the co-initiator here primarily because NPG exhibits little influence on the kinetics,[22] within the limiting of experiment errors. To be noted that various other chemicals such as mercaptobenzothiazole and *N*-methyl-*N,N*-diethanolamine are also available as the co-initiator.

Kinetics. As shown in Fig. 1(a), when the KCD content rises up from 0.3×10^{-3} to 1.4×10^{-3} mol/L, both photopolymerization rate, R_P, and double bond conversion, α increase. The maximum R_P and overall α increase by 73% (*i.e.,* from 4.5 to 7.8 s^{-1}) and 22% (*i.e.,* from 60% to 73%), respectively. However, further increasing the KCD concentration leads to a considerable diminishment for both R_P and α. Once the KCD concentration reaches 11.0×10^{-3} mol/L, the kinetic profile is quite similar to that for the mixture containing 0.3×10^{-3} mol/L of KCD, though the KCD concentration rises by 35.7 times. No significant variation on the kinetics is observable when the KCD concentration is higher than 13.7×10^{-3} mol/L.
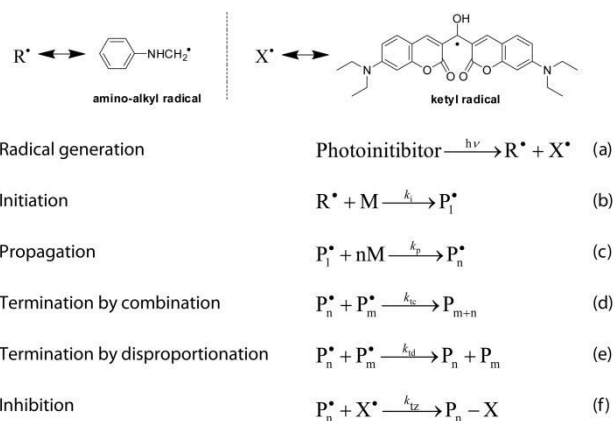
Scheme 2 Elementary Reaction Steps for the Free Radical Photopolymerization Involving the Photoinitibitor Composited of KCD and NPG.

To get a deeper insight into the photopolymerization kinetics, we list the six major elementary reaction steps in Scheme 2. Namely, (a) generating amino-alkyl radicals ($R^\bullet$) for initiation and ketyl radicals ($X^\bullet$) for inhibition respectively upon light exposure, (b) initiation, (c) chain propagation, (d) termination by bimolecular

combination of polymeric radicals, (e) termination by disproportionation of two polymeric radicals, and (f) inhibition of polymeric radicals by ketyl radicals.

Taking into account the pseudo-steady state assumption, the concentration for each type of radicals is constant and the initiation rate R_i equals the termination rate, as described by the following equations,

$$\partial[\mathrm{R}^\bullet]/\partial t = R_i - (k_{tc} + k_{td})[\mathrm{R}^\bullet]^2 - k_{tz}[\mathrm{R}^\bullet][\mathrm{X}^\bullet] \approx 0 \qquad (1)$$

$$\partial[\mathrm{X}^\bullet]/\partial t = R_i - k_{tz}[\mathrm{R}^\bullet][\mathrm{X}^\bullet] \approx 0 \qquad (2)$$

where, k_{tc}, k_{td}, k_{tz} are respectively the reaction rate constants in the steps of combination termination, disproportionation termination and inhibition. As the total concentration of initiating radicals is expected to equal that of inhibition radicals, in line with the elementary reaction step (a) in Scheme 2, the concentration for each type can be written as equation 3 by solving the equations 1 and 2,

$$[\mathrm{X}^\bullet] = [\mathrm{R}^\bullet] = (R_i/k_t)^{1/2} \qquad (3)$$

where $k_t = k_{tc} + k_{td} + k_{tz}$. Then, the polymerization rate can be given as,

$$R_p = d\alpha/dt = k_p(1-\alpha)[\mathrm{R}^\bullet] = k_p(1-\alpha)(R_i/k_t)^{1/2} \qquad (4)$$

For photopolymerization, the initiation rate R_i can be expressed as the product of initiating efficiency, ϕ, times the absorbed light intensity I_a,

$$R_i = \phi I_a \qquad (5)$$

In light of the Beer-Lambert Law, the absorbed light intensity with unites of mol/(L·s) at varied KCD concentrations can be given as,[56]

$$I_a = 2.3\varepsilon[\mathrm{KCD}]I_0 \exp(-2.3\varepsilon[\mathrm{KCD}]D)\lambda/(N_a hc) \qquad (6)$$

where, ε is the molar extinction coefficient equaling 61954 L/(mol·cm) for KCD when the light wavelength λ is 442 nm, N_a is the Avogadro's number (6.02×10²³ mol⁻¹), h is the Planck's constant (6.63×10⁻³⁴ J·s), c is the light speed (3×10⁸ m/s), I_0 is the light intensity reaching the top sample surface (20 mW/cm²), and D is the sample thickness. $\lambda/(N_a hc)$ is employed here to convert the light intensity in units of mW/cm² to the units of Einstein/(cm²·s).[56] By inserting equations 5 and 6 into the equation 4, we obtain the KCD concentration dependent photopolymerization rate as equation 7,

$$R_p = k_p(1-\alpha)\left(\frac{2.3\varepsilon[\mathrm{KCD}]I_0\phi}{k_t}\frac{\lambda}{N_a hc}\exp(-2.3\varepsilon[\mathrm{KCD}]D)\right)^{1/2} \qquad (7)$$

The equation 7 displayed here clearly shows that the photopolymerization kinetics involving photoinitibitor is the same as that for classical photo-mediated polymerizations, and the photopolymerization rate is proportional to the square root of light

intensity, as observed previously.[22, 23] When the KCD concentration is very small, a simplified expression for the equation 7 is valid,

$$R_p = k_p(1-\alpha)\left(\frac{2.3\varepsilon[\mathrm{KCD}]I_0\phi}{k_t}\frac{\lambda}{N_a hc}\right)^{1/2} \qquad (8)$$

In such cases, the photopolymerization rate for a given double bond conversion is proportional to the square root of KCD concentration, in quantitative agreement with the fitted curve 1 in Fig. 1(b). The inset in Fig. 1(b) gives a much clearer picture of the linear relationship between reaction rate and square root of KCD concentration, when the KCD content is smaller than 1.4×10⁻³ mol/L.

It is a different situation once the KCD content is higher than 1.4×10⁻³ mol/L, as it is no longer valid to ignore the effect of sample thickness. In such cases, the detected polymerization rate by P-DSC is an average value of reaction rates at different depths, which can be obtained by integrating the equation 7 over the simple thickness D and then dividing by D,[56]

$$\bar{R}_p = 2k_p(1-\alpha)\left(\frac{\phi I_0}{2.3\varepsilon[\mathrm{KCD}]k_t}\frac{\lambda}{N_a hc}\right)^{1/2}\left(\frac{1-\exp(-2.3\varepsilon[\mathrm{A}]D/2)}{D}\right) \qquad (9)$$

A plausible fitting with equation 9 on the experiment data is given in Fig. 1(b) as the fitted curve 2, implying the theory correctness. Values of 0.06 and 0.14 for $\phi^{1/2}k_p/k_t^{1/2}$ are given in the fitted curve 1 and 2, separately, implying that the initiation efficiency increases around 1.5 times for a given light intensity when increasing the KCD content. Thus, we may conclude that ketyl radical inhibition, rather than initiation rate decay that is caused by depressed Beer-Lambert light absorption, accounts for the depressed reaction kinetics at a high loading level of KCD, although they both exhibit similar effects on decreasing the concentration of propagating radicals.

Gelation. Photoinitibitor is also able to tune the photopolymerization gelation. To achieve a deeper insight into the control mechanism, we implemented the KCD concentration dependent photorheology experiments. As displayed in Fig. 2(a), both storage (G′) and loss (G″) moduli almost keep constant in the first 50 seconds although the reaction occurs once the irradiation starts, and the mixtures exhibit liquid behaviors because the G″ is much higher than the G′. As the reactions go on, both G′ and G″ increase, and they rise dramatically once the systems approach gel points. Once gels occur, G′ becomes larger than G″, and the mixtures exhibit solid-like behaviors. The crossover of G′ and G″ profiles is regarded as the gel point.[19, 57] It is clear that there is no significant change on the photorheology profiles when the KCD content is lower than 2.8×10⁻³ mol/L, though the KCD concentration increases around 10 times. A further increase of the KCD concentration leads to a prolonged gelation.

Fig. 2(b) illustrates a much clearer picture for the KCD content influence on the gelation time. When the KCD content is less than 1.8 ×10⁻³ mol/L, the gelation time of 67 s seems not to change, within the experimental errors. When the KCD rises up from 1.8 ×10⁻³ to 5.5 ×10⁻³ mol/L, the gelation time slightly increases by 21.7%. Interestingly, the gelation time almost linearly increases by 3.1 times (*i.e.*, from 84 to 345 s) when raising the KCD concentration from 5.5×10⁻³ to 21.8×10⁻³ mol/L. During the photopolymerization using traditional initiators that generate only

one type of radicals, the gelation time is usually observed to be drastically reduced with an increase of initiator concentrations (*e.g.*, 0~10 wt%), because of the increased initiating rate,[58, 59] implying that the gelation behavior led by the photoinitibitor is distinct and exceptional.
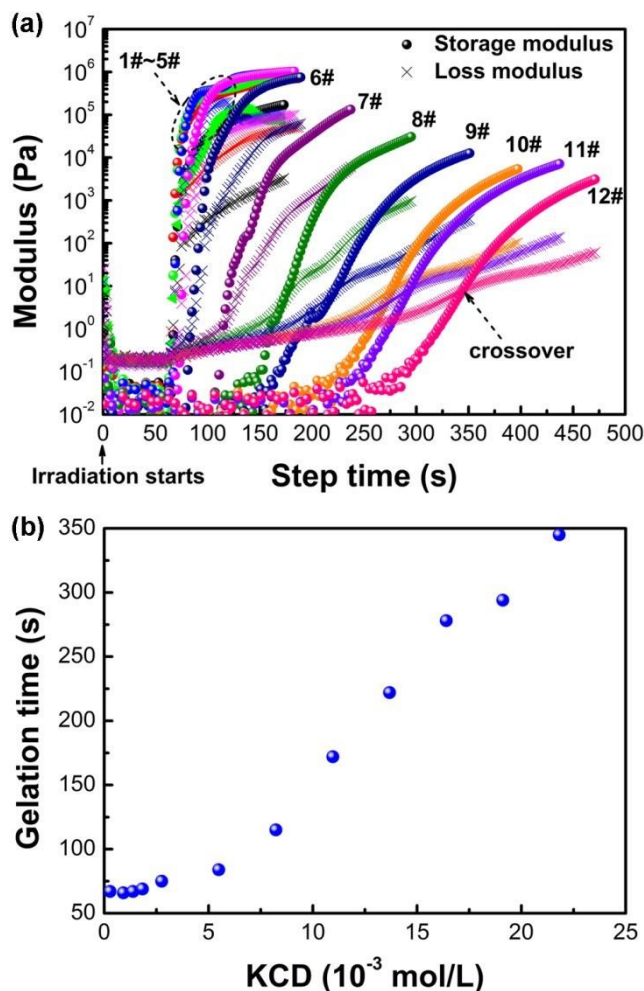

Fig. 2 (a) Storage (G′) and loss moduli (G″) versus step time during photopolymerization at different KCD concentrations. The crossover of G′ and G″ was determined as the gel point.[19, 57] KCD concentrations for each entry are listed in Table 1. (b) Gelation time as a function of KCD concentration, which implies that the augment of KCD significantly prolongs the photopolymerization gelation.

Gelation is a process functionally capable of converting small functional monomers to infinite networks that are highly cross-linked and insoluble in any solvents. Based on Flory-Stockmayer criterion,[60, 61] the theoretical monomer conversion at gel point, α_c is only determined by the monomer functionality f (in chain growth, the functionality is two times larger than the number of double bonds) with an assumption of no cyclization,

$$\alpha_c = 1/(f-1) \qquad (10)$$

It is indicative that the critical conversion at gel point is independent of the concentration of initiating radicals. The

insensitivity of gel point conversion on the initiating radical concentration is also observed by Naghash and co-workers,[62] and Wang and co-workers.[63] Hence, faster reaction is supposed to offer shorter gelation time. However, several counterintuitive results are obvious comparing the kinetics data in Fig. 1 to the gelation data in Fig. 2. Firstly, when the KCD content rises up from 0.3×10^{-3} to 1.4×10^{-3} mol/L, the maximum R_P and overall α increase by 73% and 22%, respectively, but the gelation time does not change. Secondly, the kinetic profiles are quite similar to each other for the mixtures with 0.3×10^{-3} and 11.0×10^{-3} mol/L of KCD, while the gelation time for the latter is 2.6 times larger than that for the former. Finally, no significant kinetics change is observed when the KCD concentration increases from 13.7×10^{-3} to 21.8×10^{-3} mol/L, nevertheless, the gelation time rises up from 222 to 345 s. It is reasonable to conclude that the kinetics understanding is insufficient to interpret the counterintuitive gelation data.

According to Flory's theory,[64] there exists the following criterion when the polymerization involving cross-linking reaches the gel point:

$$\rho \bar{r}_w = 1 \qquad (11)$$

where $\bar{r}_w$ is the weight-average chain length, and ρ is the cross-link density. The cross-link density can be expressed as the product of double bond conversion, α_2, and functionality, f, of monomers with a functionality larger than 2, with an equal monomer reactivity assumption,

$$\rho = -(f/2)[1 + (1/\alpha_2)\ln(1-\alpha_2)] \qquad (12)$$

It is clear that the cross-link density is insensitive to the rate of initiation as the critical monomer conversion is independent of the initiation rate. Several reports support this statement. For instances, Naghash and co-workers have disclosed that the critical weight-average molecular weight doesn't rely on the rate of initiation, leading to an initiator-independent monomer conversion at the gel point.[62] Wang and co-workers have also found out that the cross-link density is independent of the initiating radical concentration, while highly dependent on the initial divinyl monomer concentration and monomer conversion in the RAFT copolymerization of vinyl/divinyl systems.[63] As the photopolymerization proceeds, $\rho \bar{r}_w$ gradually increases from zero to 1, and no gelation occur until the value approaches 1. To postpone gelation, a drastic decrease in the chain length is required.[64] Ketyl radical inhibition leads to the formation of shortened polymer chains as shown in Scheme 3, comparing to the bimolecular termination step of propagating radicals. Hence, the weight-average chain length, $\bar{r}_w$ is expected to be diminished when increasing the KCD content, and higher double bond conversion is required to form a gel with an infinite polymer network structure. The linear relationship between α_c and the reciprocal of $\bar{r}_w$ at the gel point was also theoretically deduced by Okay using the method of moments.[65] As such, the cross-link density of the formed gel is envisioned to be increased on the basis of equation 12, which is evidenced by the increased storage modulus, G′ from 1 to 8 Pa, according the rubbery elastic theory.[66]

Because of the increased double bond conversion at gel point with an increase of KCD content, the increased reaction rate leads to an unchanged gelation time when the KCD content is less than 1.4×10^{-3} mol/L; reversely, once the KCD content is larger than 1.4×10^{-3} mol/L, the decreased polymerization rate results in prolonged gelation.

repeating unit
propagating radical
inhibiting radical
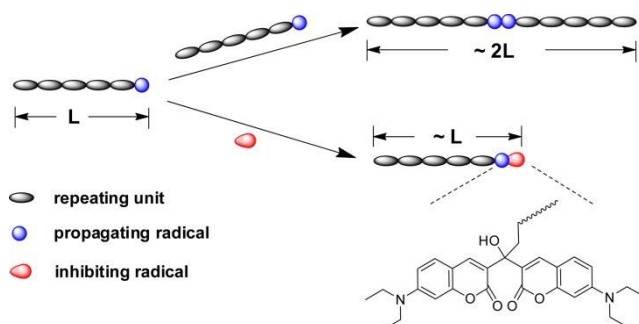
Scheme 3 Illustration for the Shortened Polymer Chain Length by Ketyl Radical Inhibition.

Boltzmann equation:
$$y = y_2 + (y_1 - y_2)/[1 + \exp((x - x_0)/dx)]$$
$y_1 = -67.2$
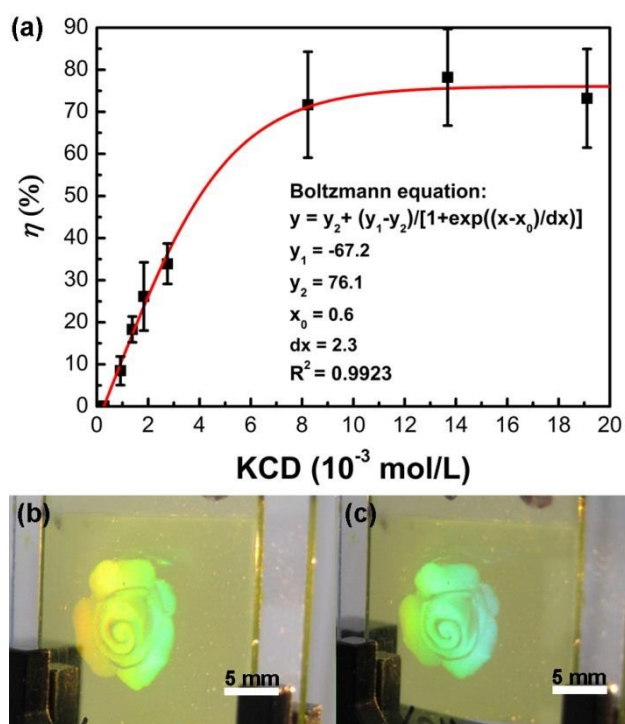$y_2 = 76.1$
$x_0 = 0.6$
$dx = 2.3$
$R^2 = 0.9923$

Fig. 3 (a) KCD concentration dependent diffraction efficiency, η, indicating that ketyl radical inhibition is profitable to enhance the holographic performances. (b), (c) Colored 3D images in the form of H-PDLCs that are readily identifiable to the naked eye under tungsten light illumination.

Phase segregation and electro-optical performances. Recently, we disclosed that the photoinitibitor was able to enhance the phase separation and grating diffraction.[22, 23] However, since the photopolymerization was depressed in these seminal studies, a question may be raised whether one is able to achieve good

gratings by lowering down the KCD content to less than 1.4×10^{-3} mol/L as the photopolymerization kinetics is observed to be depressed as well. To answer this question, we further implemented holography and electro-optical characterization. We choose H-PDLCs here primarily because compared with holographic photopolymer/nanoparticles composites, H-PDLCs gratings are able to exhibit intriguing morphology dependent responses upon external electric stimulus, and thus to offer deeper information about the degree of phase separation based on the fundamental structure-property relationship.

The KCD concentration dependent diffraction efficiency η is shown in Fig. 3(a). As displayed, no obvious gratings form when the KCD concentration is lower than 0.3×10^{-3} mol/L. With an augment of the KCD content, the diffraction efficiency gradually steps toward the maximum diffraction efficiency of 78±11%. The well-fitted curve, which overlays over the data using a Boltzmann equation, is a clear guide to predict the diffraction efficiency at varied KCD concentrations, whereby we may know that detectable gratings are able to form when the KCD content is larger than the critical value of 0.6×10^{-3} mol/L. As expected, the entry with 1.4×10^{-3} mol/L with the highest reaction rate is not able to afford desired gratings probably due to the fast gelation as mentioned above. Adding classical radical retarders and/or inhibitors,[23] or decreasing light intensity in traditional photoinitiating systems,[22] is an efficient technique to depress the photopolymerization yet has been evidenced to be incapable of offering desirable holographic gratings. Thus, it is reasonable to interpret that a relatively high reaction rate is required to facilitate component diffusion during holographic recording. We are also able to conclude that the photoinitibitor, by virtue of photo-mediated initiation and ketyl radical inhibition, is a unique and distinct approach to enhance the holographic phase separation structure. Although better gratings can be formed by decreasing the light intensity when using the photoinitibitor composed of KCD and NPG,[23] gelation time delay, rather than initiating rate decrease plays the predominant role on enhancing the phase separation structure and holographic performances. For instance, comparing the entries with 0.3×10^{-3} and 8.2×10^{-3} mol/L of KCD with similar reaction kinetics profiles, the former is unable to offer satisfactory gratings while the latter affords fine holograms with high diffraction efficiency. Because of the high diffraction efficiency of H-PDLCs gratings when the KCD content is larger than 8.2×10^{-3} mol/L, colored 3D images that are readily recognized without using polarized glasses, as visualized in Figs. 3(b) and 3(c), are easily fabricated.

Since scaffolding morphologies are formed in these gratings, as depicted in the inset of Fig. 4, no LCs droplets can be observed, in good agreement with that reported previously.[46] To further understand the KCD content dependent phase separation, we calculated the segregation degree, SD, using the method we recently employed.[23] Average refractive indices of 1.59[22] and 1.50 for LCs and polymer were utilized to implement the calculation, respectively. For the holographic photopolymer/ZnS nanoparticles composites, through introducing a constant β, we successfully deduced an equation that well described the SD as a function of

the ratio of gelation time t_{gel} to mixture viscosity ν, on the basis of Fick's second Law,[23]

$$SD = SD_{max}\left[1 - e^{-\beta(t_{gel}/\nu)}\right] \tag{13}$$

In the current situation for H-PDLCs with varied KCD concentrations, the mixture viscosity is supposed to be constant since less than 1 wt% of KCD are added. We plotted the SD as a function of gelation time in Fig. 4.
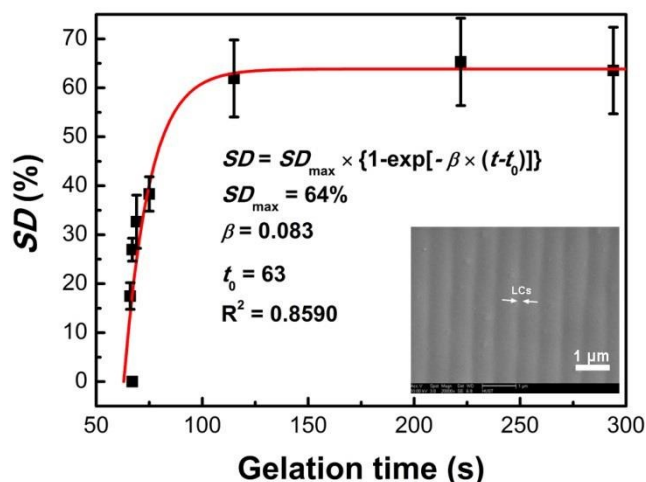

Fig. 4. The segregation degree, *SD*, versus gelation time that was afforded by varying the KCD concentrations, which implies that there is an induction time for phase separation in H-PDLCs gratings. Inset: a SEM image for the H-PDLCs gratings after removing LCs *via* hexane extraction.

As visualized, no phase separation takes place once the gelation time is less than 66 s, and then the SD steeply increases with an augment of gelation time. The SD value approaches 95% of the maximum at 99 s, and finally levels off at 64%. The SD value of 64% is plausible for H-PDLCs gratings with a diffraction efficiency of 78% according to the previously work from Sutherland and co-workers.[67] It is interesting that the equation 13 is no longer applicable to describe $SD \sim t_{gel}$ relationship during the formation of H-PDLCs gratings. Rewriting the equation 13 by incorporating another constant t_0, we are able to achieve a well-fitted curve that is overlaid over the data,

$$SD = SD_{max}\left\{1 - \exp\left[-\beta\left(t - t_0\right)\right]\right\} \tag{14}$$

The constant t_0 is given as 63 s, indicating that there is an induction time before which no detectable phase separation occurs, which is quite different from that observed in holographic photopolymer/ZnS nanoparticles composites.[23] During the formation of H-PDLCs grating, monomer and LCs diffusion, LCs nucleation and polymerization gelation occur as the photopolymerization proceeds, only the diffusion time is much smaller than the nucleation time, and the latter is much shorter than the gelation time, can a fine grating with completed phase separation be afforded.[47] As such, the induction time required to start the phase separation probably corresponds to the time needed for sufficient LC nucleation. The equations 13 and 14 clearly provide the answer to the longstanding question of how to improve the holographic performances *via* formulations optimization, *i.e.*, *via* tuning the photopolymerization gelation time and mixture viscosity.

Because of the intriguing responsive capability of H-PDLCs gratings to external electric fields, we are able to achieve a deeper insight into the degree of phase separation by measuring the driving voltage. In general, a sinusoidal distribution of material yields in the H-PDLCs gratings after holographic recording, with a random orientation of the nematic directors in small LCs domains. In the turn-off state, the refractive index of LCs is much higher than that for aliphatic acrylate polymer, resulting in a strong diffraction once a probe beam irradiates the H-PDLCs gratings at the Bragg angle. The diffraction efficiency primarily depends on the refractive index difference between the polymer-rich domains and LCs-rich areas, as well as the volume ratio of LCs within the LCs-rich channels, in light of the Kogelnik's coupling coefficient.[67] In such cases, the improved phase separation is envisioned to offer enhanced diffraction efficiency. Reversely, once we apply a suitable voltage to turn on the H-PDLCs gratings, the nematic directors of LCs with positive dielectric constants tend to align along with the electric field, resulting in a refractive index match between the polymer and LCs, and thus a decrease of diffraction efficiency, as shown in the inset of Fig. 5.
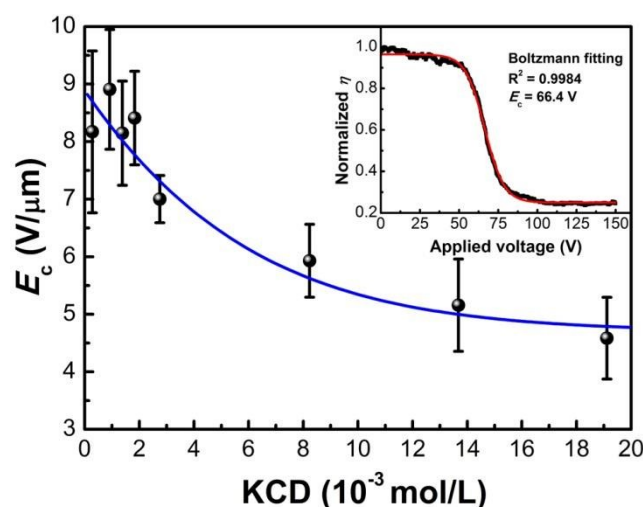

Fig. 5 Critical driving voltage E_c versus KCD concentration, indicating that increasing the KCD loading gradually decreases the critical driving voltage. Inset: a representative electro-optical responsive curve used to measure the E_c of H-PDLCs gratings

Since the scaffolding morphology without LCs droplets is given in this text, as depicted in the inset of Fig. 4, it is reasonable to characterize the electro-optical performances using the method proposed by Crawford and co-workers,[68] whereby the critical driving voltage E_c is related to the interface interaction between polymer and LCs,[68]

$$E_c = \left[\frac{4\pi^2 K}{\Lambda^2 \varepsilon_0 |\Delta\varepsilon|} + \frac{A}{\varepsilon_0 |\Delta\varepsilon|}\right]^{1/2} \tag{15}$$

where, K is the average elastic constant to be assumed as 10^{-11} N,[68] and $\Delta\varepsilon$ is the dielectric anisotropy that is reported to be 11.5 for the nematic LCs P0616A used here. ε_0 is the vacuum permittivity approximating to 8.85×10^{-12} F/N, Λ is the grating period with a value of 827 nm. A is a parameter that is used to express the interface interaction with units of J/m^3. $4\pi^2 K/\left(\Lambda^2\varepsilon_0\left|\Delta\varepsilon\right|\right)$ is the critical voltage that is needed to enable the Frederiks transition of pure LCs, at which an abrupt change of optical properties can be observed. To obtain the E_c after which a drastic decrease of grating diffraction is noted, we employed Boltzmann fitting on the electro-optical response curves. Reasonable values are afforded by the fitting, as illustrated in the inset of Fig. 5. Then we plotted the E_c as a function of KCD concentration in Fig. 5. As clearly displayed, the E_c of H-PDLCs gratings gradually decreases by 43% (*i.e.*, from 8.9 ± 1.0 to 4.6 ± 0.7 V/μm) as a whole when increasing the KCD content, although no significant change is observed when the KCD content is less than 1.8×10^{-3} mol/L, indicating a decrease of the interface interaction parameter. It is plausible that the enhanced phase separation leads to a decrease of interacting surface area between polymer and LCs, consequently results in a decrease of total anchoring energy. If we assume that the interface interaction parameter A decreases exponentially with an augment of KCD concentration, we can obtain a good data fitting to describe the relationship between E_c and KCD content, using the following equation,

$$A=493+57\exp(-216[\text{KCD}])\tag{16}$$

the slightly larger number of A than that reported elsewhere (400 J/m³)[68] means that the polymer used here is able to offer a stronger interface anchoring energy. The drastic decrease of E_c and A can be reasonable signals to show the enhanced phase separation *via* ketyl radical inhibition when increasing the KCD content. It is worth mentioning that the hyperbranched monomer employed in this study also plays an important role in decreasing the driving voltage when increasing the KCD content *via* providing non-droplet scaffolding morphological H-PDLCs. Increased driving voltage in H-PDLCs with droplet-morphology when increasing the KCD content has been observed.[22] The significantly improved phase separation of holographic gratings is of essential importance for reconstructing colored 3D images with high-brightness that are easily recognized by the naked eye,[22, 23] as displayed in Figs. 3(b) and 3(c), opening up the excellent possibilities on the commercialization of glasses-free 3D image tags for advanced anticounterfeiting and stereo-advertisements.

Conclusions

In summary, we employed a systematical study on the photoinitibitor concentration-dependent photopolymerization kinetics, gelation, phase separation and electro-optical behaviors of H-PDLCs gratings when varying the KCD concentration from 0.3×10^{-3} to 21.8×10^{-3} mol/L. Both polymerization rate R_P and double bond conversion α increased when the KCD content rose up from 0.3×10^{-3} to 1.4×10^{-3} mol/L. However, both R_P and α then considerably decreased when further increasing the KCD loading. Once the

KCD concentration reached 11.0×10^{-3} mol/L, the maximum R_P and overall α were almost the same as those for the mixture containing 0.3×10^{-3} mol/L of KCD, individually, although the KCD concentration rose by 35.7 times. No significant variation of the kinetics was observable when the KCD concentration was higher than 13.7×10^{-3} mol/L. Numerical expressions were successfully deduced to describe the photopolymerization kinetics, implying that the reaction kinetics afforded by the photoinitibitor complied with the classical photopolymerization kinetics characteristics in the full range of KCD concentrations. Meanwhile, as the KCD content increased, the initiation efficiency was calculated to rise 1.5 times, suggesting that the depressed photopolymerization kinetics was caused by the ketyl radical inhibition, rather than decreased Beer-Lambert absorption. Counterintuitively, no variation of the gelation time was detected when the KCD content was less than 1.8×10^{-3} mol/L, while the gelation time dramatically increased by 4.1 times when raising the KCD loading from 1.8×10^{-3} to 21.8×10^{-3} mol/L. The exceptional behavior compared to other initiating systems was attributed to the ketyl radical inhibition that consequently resulted in shortened weight-average chain lengths and increased gel point conversions. With an augment of KCD content from 0.3×10^{-3} to 8.2×10^{-3} mol/L, the segregation degree of H-PDLCs gratings increased from zero to 64%, and the diffraction efficiency of holograms rose from zero to $78\pm11\%$. No significant variations of both segregation and diffraction efficiency were observed when further increasing the KCD content. A significant decrease of the driving voltage in the scaffolding morphological H-PDLCs was also achieved when increasing the KCD content because of the increased phase separation and the consequently decreased interface interaction. This study outlines a fundamental principle to design desirable holograms that, one should pay primary attention to the control over formulation gelation and viscosity, other than the kinetics concern. The easily fabricated colored 3D images to the naked eye by using the photoinitibitor also open up perspectives on the application of 3D holograms for advanced anticounterfeiting and stereo-advertisements.

## Acknowledgements

Conflict of interest

The authors declare no competing financial interest.

Notes and references

1. A. B. Scranton, C. N. Bowman and R. W. Peiffer, *Photopolymerization-Fundamentals and Applications*, American Chemical Society, Washington, DC, 1996.
2. S. Chatani, C. J. Kloxin and C. N. Bowman, *Polym. Chem.*, 2014, **5**, 2187-2201.
3. C. E. Hoyle and C. N. Bowman, *Angew. Chem., Int. Ed.*, 2010, **49**, 1540-1573.
4. N. Gupta, B. F. Lin, L. Campos, M. D. Dimitriou, S. T. Hikita, N. D. Treat, M. V. Tirrell, D. O. Clegg, E. J. Kramer and C. J. Hawker, *Nat. Chem.*, 2010, **2**, 138-145.
5. M. A. Tasdelen and Y. Yagci, *Angew. Chem., Int. Ed.*, 2013, **52**, 5930-5938.
6. J. O. Mueller, N. K. Guimard, K. K. Oehlenschlaeger, F. G. Schmidt and C. Barner-Kowollik, *Polym. Chem.*, 2014, **5**, 1447-1456.
7. O. Altintas, M. Glassner, C. Rodriguez-Emmenegger, A. Welle, V. Trouillet and C. Barner-Kowollik, *Angew. Chem., Int. Ed.*, 2015, **54**, 5777-5783.
8. S. Dadashi-Silab, C. Aydogan and Y. Yagci, *Polym. Chem.*, 2015, **6**, 6595-6615
9. J. R. Tumbleston, D. Shirvanyants, N. Ermoshkin, R. Januszewicz, A. R. Johnson, D. Kelly, K. Chen, R. Pinschmidt, J. P. Rolland, A. Ermoshkin, E. T. Samulski and J. M. DeSimone, *Science*, 2015, **347**, 1349-1352.
10. A. R. Schultz, P. M. Lambert, N. A. Chartrain, D. M. Ruohoniemi, Z. Zhang, C. Jangu, M. Zhang, C. B. Williams and T. E. Long, *ACS Macro Lett.*, 2014, **3**, 1205-1209.
11. B. P. Fors and C. J. Hawker, *Angew. Chem., Int. Ed.*, 2012, **51**, 8850-8853.
12. A. Ohtsuki, L. Lei, M. Tanishima, A. Goto and H. Kaji, *J. Am. Chem. Soc.*, 2015, **137**, 5610-5617.
13. J. E. Poelma, B. P. Fors, G. F. Meyers, J. W. Kramer and C. J. Hawker, *Angew. Chem., Int. Ed.*, 2013, **52**, 6844-6848.
14. R. Nazir, E. Balčiūnas, D. Buczyńska, F. Bourquard, D. Kowalska, D. Gray, S. Maćkowski, M. Farsari and D. T. Gryko, *Macromolecules*, 2015, **48**, 2466-2472.
15. W. X. Xi, H. Y. Peng, A. Aguirre-Soto, C. J. Kloxin, J. W. Stansbury and C. N. Bowman, *Macromolecules*, 2014, **47**, 6159-6165.
16. T. Gong, B. J. Adzima, N. H. Baker and C. N. Bowman, *Adv. Mater.*, 2013, **25**, 2024-2028.
17. H. Y. Peng, D. P. Nair, B. A. Kowalski, W. X. Xi, T. Gong, C. Wang, M. Cole, N. B. Cramer, X. L. Xie, R. R. McLeod and C. N. Bowman, *Macromolecules*, 2014, **47**, 2306-2315.
18. H. Y. Peng, C. Wang, W. X. Xi, B. A. Kowalski, T. Gong, X. L. Xie, W. T. Wang, D. P. Nair, R. R. McLeod and C. N. Bowman, *Chem. Mater.*, 2014, **26**, 6819-6826.
19. T. F. Scott, B. A. Kowalski, A. C. Sullivan, C. N. Bowman and R. R. McLeod, *Science*, 2009, **324**, 913-917.
20. J. Fischer and M. Wegener, *Laser Photon. Rev.*, 2013, **7**, 22-44.
21. Z. Gan, Y. Cao, R. A. Evans and M. Gu, *Nat. Commun.*, 2013, **4**, 2061.
22. H. Y. Peng, S. G. Bi, M. L. Ni, X. L. Xie, Y. G. Liao, X. P. Zhou, Z. G. Xue, J. T. Zhu, Y. Wei, C. N. Bowman and Y.-W. Mai, *J. Am. Chem. Soc.*, 2014, **136**, 8855-8858.
23. M. L. Ni, H. Y. Peng, Y. G. Liao, Z. F. Yang, Z. G. Xue and X. L. Xie, *Macromolecules*, 2015, **48**, 2958-2966.
24. S. C. Ligon, B. Husár, H. Wutzel, R. Holman and R. Liska, *Chem. Rev.*, 2014, **114**, 557-589.
25. Y. Yagci, S. Jockusch and N. J. Turro, *Macromolecules*, 2010, **43**, 6245-6260.
26. J. Zhao, J. Lalevee, H. Lu, R. MacQueen, S. H. Kable, T. W. Schmidt, M. H. Stenzel and P. Xiao, *Polym. Chem.*, 2015, **6**, 5053-5061.
27. P. Xiao, F. Dumur, M. Frigoli, M.-A. Tehfe, B. Graff, J. P. Fouassier, D. Gigmes and J. Lalevée, *Polym. Chem.*, 2013, **4**, 5440-5448.
28. J. P. Fouassier, X. Allonas and D. Burget, *Prog. Org. Coat.*, 2003, **47**, 16-36.
29. D. A. Parthenopoulos and P. M. Rentzepis, *Science*, 1989, **245**, 843-845.
30. F.-K. Bruder, R. Hagen, T. Rölle, M.-S. Weiser and T. Fäcke, *Angew. Chem., Int. Ed.*, 2011, **50**, 4552-4573.
31. M. Ozaki, J.-i. Kato and S. Kawata, *Science*, 2011, **332**, 218-220.
32. D. E. Smalley, Q. Y. J. Smithwick, V. M. Bove, J. Barabas and S. Jolly, *Nature*, 2013, **498**, 313-317.
33. P. A. Blanche, A. Bablumian, R. Voorakaranam, C. Christenson, W. Lin, T. Gu, D. Flores, P. Wang, W. Y. Hsieh, M. Kathaperumal, B. Rachwal, O. Siddiqui, J. Thomas, R. A. Norwood, M. Yamamoto and N. Peyghambarian, *Nature*, 2010, **468**, 80-83.
34. K. Liu, H. Xu, H. Hu, Q. Gan and A. N. Cartwright, *Adv. Mater.*, 2012, **24**, 1604-1609.
35. A. K. Yetisen, I. Naydenova, F. da Cruz Vasconcellos, J. Blyth and C. R. Lowe, *Chem. Rev.*, 2014, **114**, 10654-10696.
36. R. L. Sutherland, L. V. Natarajan, V. P. Tondiglia and T. J. Bunning, *Chem. Mater.*, 1993, **5**, 1533-1538.
37. T. J. Bunning, L. V. Natarajan, V. P. Tondiglia and R. L. Sutherland, *Annu. Rev. Mater. Sci.*, 2000, **30**, 83-115.
38. S. J. Woltman, G. D. Jay and G. P. Crawford, *Nat. Mater.*, 2007, **6**, 929-938.
39. W. B. Huang, L. S. Chen and L. Xuan, *RSC Adv.*, 2014, **4**, 38606-38613.
40. L. J. Liu, L. Xuan, G. Y. Zhang, M. H. Liu, L. F. Hu, Y. G. Liu and J. Ma, *J. Mater. Chem. C*, 2015, **3**, 5566-5572.
41. A. Urbas, V. Tondiglia, L. Natarajan, R. Sutherland, H. P. Yu, J. H. Li and T. Bunning, *J. Am. Chem. Soc.*, 2004, **126**, 13580-13581.
42. C. Sanchez, M. J. Escuti, C. van Heesch, C. W. M. Bastiaansen and D. J. Broer, *Appl. Phys. Lett.*, 2005, **87**, 094101.
43. M. S. Park, E. H. Kim and B. K. Kim, *J. Polym. Eng.*, 2008, **28**, 169-178.
44. L. V. Natarajan, C. K. Shepherd, D. M. Brandelik, R. L. Sutherland, S. Chandra, V. P. Tondiglia, D. Tomlin and T. J. Bunning, *Chem. Mater.*, 2003, **15**, 2477-2484.
45. T. J. White, L. V. Natarajan, V. P. Tondiglia, P. F. Lloyd, T. J. Bunning and C. A. Guymon, *Macromolecules*, 2007, **40**, 1121-1127.
46. H. Y. Peng, M. L. Ni, S. G. Bi, Y. G. Liao and X. L. Xie, *RSC Adv.*, 2014, **4**, 4420-4426.
47. T. J. Bunning, L. V. Natarajan, V. P. Tondiglia, R. L. Sutherland, R. Haaga and W. W. Adams, *Proc. SPIE*, 1996, **2651**, 44-55.
48. M. De Sarkar, N. L. Gill, J. B. Whitehead and G. P. Crawford, *Macromolecules*, 2003, **36**, 630-638.
49. W. B. Huang, D. L. Pu, S. Shen, G. J. Wei, L. Xuan and L. S. Chen, *J. Phys. D-Appl. Phys.*, 2015, **48**, 375303.
50. W. Huang, Y. Liu, Z. Diao, C. Yang, L. Yao, J. Ma and L. Xuan, *Appl. Opt.*, 2012, **51**, 4013-4020.
51. J. Y. Woo and B. K. Kim, *ChemPhysChem*, 2007, **8**, 175-180.
52. J. Klosterman, L. V. Natarajan, V. P. Tondiglia, R. L. Sutherland, T. J. White, C. A. Guymon and T. J. Bunning, *Polymer*, 2004, **45**, 7213-7218.

53. Y. J. Liu, X. W. Sun, H. T. Dai, J. H. Liu and K. S. Xu, *Opt. Mater.*, 2005, **27**, 1451-1455.
54. J. Y. Woo, E. H. Kim and B. K. Kim, *ChemPhysChem*, 2008, **9**, 141-146.
55. J. Y. Woo and B. K. Kim, *Liq. Cryst.*, 2008, **35**, 987-994.
56. G. Odian, *Principles of Polymerization*, John Wiley & Sons, Inc., New York, 4th edn., 2004.
57. H. H. Winter and F. Chambon, *J. Rheol.*, 1986, **30**, 367-382.
58. A. Boddapati, S. B. Rahane, R. P. Slopek, V. Breedveld, C. L. Henderson and M. A. Grover, *Polymer*, 2011, **52**, 866-873.
59. R. P. Slopek, H. K. McKinley, C. L. Henderson and V. Breedveld, *Polymer*, 2006, **47**, 2263-2268.
60. W. H. Stockmayer, *J. Chem. Phys.*, 1943, **11**, 45-55.
61. P. J. Flory, *J. Am. Chem. Soc.*, 1941, **63**, 3083-3090.
62. H. J. Naghash, O. Okay and Y. Yağci, *Polymer*, 1997, **38**, 1187-1196.
63. R. Wang, Y. Luo, B.-G. Li and S. Zhu, *Macromolecules*, 2009, **42**, 85-94.
64. P. J. Flory, *J. Am. Chem. Soc.*, 1947, **69**, 2893-2899.
65. O. Okay, *Polymer*, 1994, **35**, 2613-2618.
66. C. J. Kloxin and C. N. Bowman, *Chem. Soc. Rev.*, 2013, **42**, 7161-7173.
67. R. L. Sutherland, L. V. Natarajan, V. P. Tondiglia, T. J. Bunning and W. W. Adams, *Proc. SPIE*, 1995, **2404**, 132-143.
68. K. K. Vardanyan, J. Qi, J. N. Eakin, M. De Sarkar and G. P. Crawford, *Appl. Phys. Lett.*, 2002, **81**, 4736-4738.

Table of Contents

shortened polymer chain   gelation delay   colored 3D image
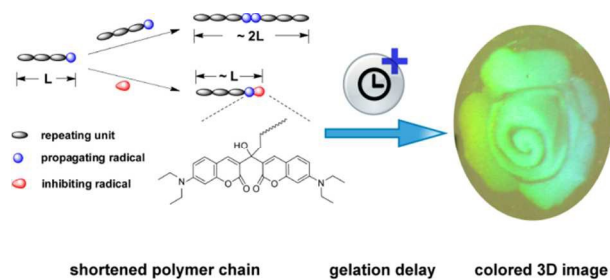
Ketyl radical inhibition results in prolonged gelation and enhanced diffraction efficiency, allowing for the facile fabrication of colored 3D images.